Supporting Information

Unusual regio-versatility of acetyltransferase Eis, a cause of drug resistance in XDR-TB

Wenjing Chen,[†] Tapan Biswas,[†] Vanessa R. Porter, Oleg V. Tsodikov,* and Sylvie Garneau-Tsodikova*

[†] *These authors contributed equally to this work*

* To whom correspondence should be addressed: E-mail: sylviegt@umich.edu or olegt@umich.edu

Content

1. Bacterial strains, plasmids, materials, and instrumentations

Restriction endonucleases, T4 DNA ligase, and Phusion DNA polymerase were bought from NEB (Ipswich, MA). DNA primers for PCR were ordered from Integrated DNA Technologies (IDT; Coralville, IA). The pET28a and pET22b vectors were purchased from Novagen (Gibbstown, NJ). The chemically competent bacterial strains *E. coli* TOP10 and BL21 (DE3) were bought from Invitrogen (Carlsbad, CA). The *Mycobacterium tuberculosis* H37Rv genomic DNA was obtained from the Biodefense & Emerging Infections Research Resources Repository (BEI resources, Manassas, VA). DNA sequencing was performed at the University of Michigan DNA Sequencing Core. Fast protein liquid chromatography (FPLC) was done as the last protein purification step on a Bio-Rad BioLogic DuoFlow (Bio-Rad, Hercules, CA) using a HighPrep^{TM} 26/60 Sephacryl^{TM} S-200 High Resolution Column (GE Healthcare, Piscataway, NJ). DTDP, acetyl-CoA, and aminoglycosides (AGs) (apramycin (APR), amikacin (AMK), hygromycin (HYG), kanamycin A (KAN), neomycin B (NEO), sisomicin (SIS), spectinomycin (SPT), streptomycin (STR), and ribostamycin (RIB)) were purchased from Sigma-Aldrich (Milwaukee, WI). The AGs neamine (NEA), netilmicin (NET), paromomycin (PAR), and tobramycin (TOB) were bought from AK Scientific (Mountain View, CA) (Fig. S1). Determination of substrate specificity by UV-Vis assays was done on a multimode SpectraMax M5 plate reader using 96-well plates (Fisher Scientific). TLCs (Merck, Silica gel 60 F_{254}) were visualized using a cerium-molybdate stain ($(NH_4)_2Ce(NO_3)_6$ (5 g), $(NH_4)_6Mo_7O_{24}•4H_4O$ (120 g), H_2SO_4 (80 mL), H_2O (720 mL)). 1,2',6'-triacetyl-NEA was purified by SiO_2 flash chromatography (Dynamic Absorbents 32-63 μ). ^{13}C NMR, DEPT, and HETCOR spectra were recorded on a Bruker Avance^{TM} 500 MHz spectrometer. ^{1}H NMR, 2D-COSY, and 2D-TOCSY spectra were recorded on a Bruker Avance III^{TM} 600 MHz spectrometer. All NMR spectra were recorded in D_2O as well as in 9:1/H_2O:D_2O (in order to identify the amide connectivity). Liquid chromatography mass spectrometry (LCMS) was performed on a Shimadzu LCMS-2019EV equipped with a SPD-20AV UV-Vis detector and a LC-20AD liquid chromatograph.

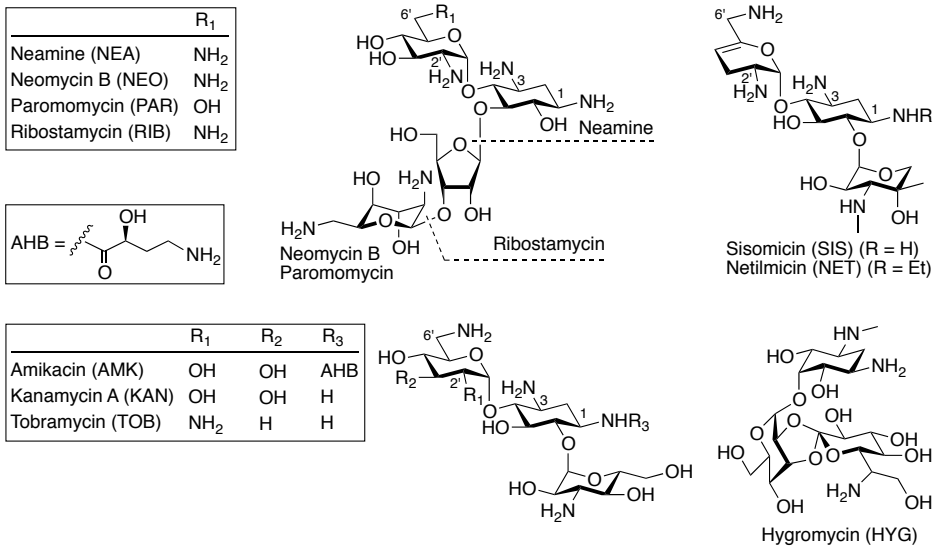

Fig. S1. Structures of AGs that are substrates of Eis.

2. BLAST and multiple sequence alignment analysis of Eis homologs

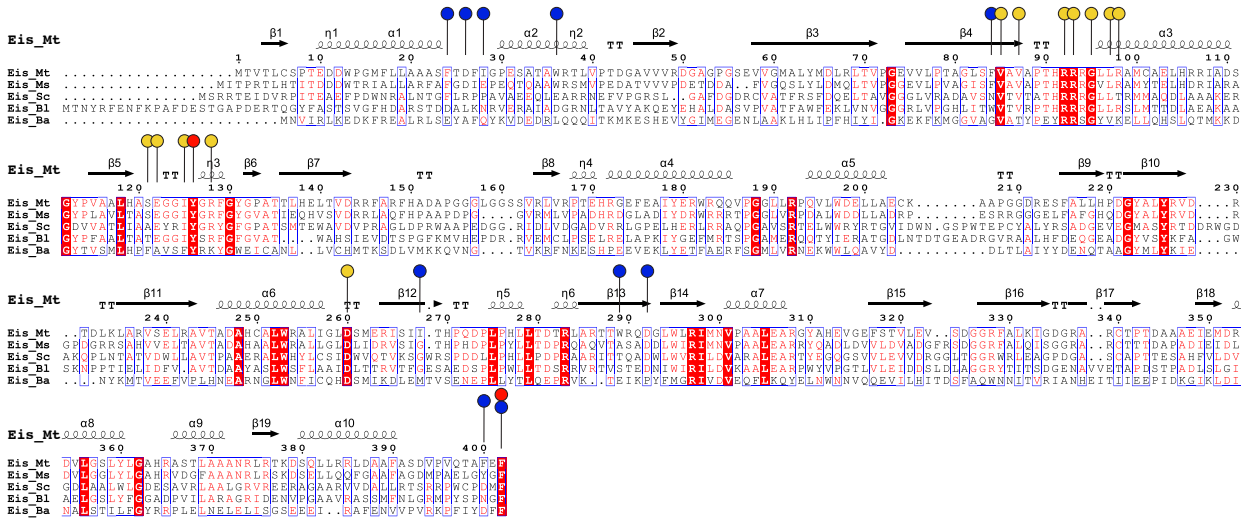

Fig. S2. Multiple sequence alignment of Eis homologs. The residues that are directly involved in the acetyl transfer are marked by red circles, those that bind CoA by yellow circles, and those that form the AG binding pocket by blue circles. The abbreviated names of bacterial species correspond to the following: *Mycobacterium tuberculosis* H37Rv (Mt), *Mycobacterium smegmatis* str. MC2 155 (Ms), *Streptomyces coelicolor* A3(2) (Sc), *Brevibacterium linens* BL2 (Bl), and *Bacillus anthracis* str. Sterne (Ba).

3. Cloning, overexpression, and purification of Eis proteins

3.1. Preparation of pEis-pET28a(NHis), pEis-pET22b(CHis), Eis single point mutant(NHis), and Eis deletion mutant(NHis) overexpression constructs

The primers used for the amplification of *eis* and mutant *eis* genes (gene locus Rv2416c) are listed in Table S1. PCRs were performed using *M. tuberculosis* H37Rv genomic DNA and

Phusion DNA polymerase (NEB, Ipswich, MA) according to the instructions provided by NEB. For the construction of the pEis-pET28a(NHis), pEis1-311-pET28a(NHis), pEis1-399-pET28a(NHis), pEis292-402-pET28a(NHis), and pEis-pET22b(CHis), the amplified *eis* genes were inserted into the linearized pET28a and pET22b vectors via the corresponding *Nde*I/*Bam*HI and *Nde*I/*Hind*III restriction sites, respectively. The single point Eis mutants were constructed using the SOE method (1). In the first round of PCR, the sequence downstream and upstream of the mutation were separately amplified using the pEis-pET28a(NHis) plasmid as a template in conjunction with the 5' primer of the *mutant* with the 3' primer for *eis(NHis)* and the 5' primer for *eis(NHis)* with the 3' primer for the *mutant*, respectively (Table S1). The resulting amplified PCR fragments were gel-purified and subjected to a second round of PCR using the forward and reverse primers for *eis(NHis)* (Table S1). The newly amplified fragments were then digested with *Nde*I and *Bam*HI and subcloned into the linearized pET28a vector via the corresponding *Nde*I/*Bam*HI restriction sites to give the single mutants F24A, F27A, I28A, W36A, F84A, V87A, R93A, H119A, S121A, Y126A, R128A, R148A, W197A, D292A, and Y310A. The plasmids encoding the above proteins were transformed into *E. coli* TOP10 chemically competent cells. The sequences of all expression clones were confirmed at the University of Michigan DNA Sequencing Core.

Table S1. Primers used for the PCR amplification of the *eis* gene from *M. tuberculosis*

gene (vector used for cloning)	5' primer	3' primer
eis(NHis) (pET28a)	CCGCGGCATATGCTACAGTCGGATTC	CTAGCAGGATCCTCAGAACTCGAACGCG
eis(CHis) (pET22b)	CCGCGGCATATGCCACAGTCGGATTC	GCACGGAAGCTTGAACTCGAACGCGGTC
eis1-311(NHis) (pET28a)	CCGCGGCATATGCTACAGTCGGATTC	CTCGCCGGATCCTCAAGCGTAACCACGCGCC
eis1-399(NHis) (pET28a)	CCGCGGCATATGCTACAGTCGGATTC	CCTTCAGGATCCTCACGCGGTCTGGACGGG
eis292-402(NHis) (pET28a)	ACCTGGCATATGGACGGCCTGTGGTTGCGC	CTAGCAGGATCCTCAGAACTCGAACGCG
eisF24A(NHis) (pET28a)	GCCGCGGCCAGTgcgACCGATTTCATC	GATGAAATCGGTcgcACTGGCCGCGGC
eisF27A(NHis) (pET28a)	CCAGTTTCACCGATGCGATCGGCCCTG	CAGGGCCGATcgcATCGGTGAAACTGG
eisI28A(NHis) (pET28a)	CACCGATTTCgcgGGCCCTGAATC	GATTCAGGGCCgcGAAATCGGTG
eisW36A(NHis) (pET28a)	CAGCGACCGCCgcgCGGACCCTGGTGCC	GGCACCAGGGTCCGcgcGGCGGTCGCTG
eisF84A(NHis) (pET28a)	GCCGGTCTCAGTgcgGTCGCGGTGGCG	CGCCACCGCGACcgcACTGAGACCGGC
eisV87A(NHis) (pET28a)	GTTTCGTCGCGgcgGCGCCGACGCATC	GATGCGTCGGCGCcgcCGCGACGAAAC
eisR93A(NHis) (pET28a)	CCGACGCATCGCgcgCGCGGCTTGCTGCGC	GCGCAGCAAGCCGCGcgcGCGATGCGTCGG
eisH119A(NHis) (pET28a)	GTCGCGGCACTGgcgGCTAGCGAGGGCGGC	GCCGCCCTCGCTAGCcgcCAGTGCCGCGAC
eisS121A(NHis) (pET28a)	GCACTGCATGCTgcgGAGGGCGGCATC	GATGCCGCCCTCcgcAGCATGCAGTGC
eisY126A(NHis) (pET28a)	GAGGGCGGCATCgcgGGCCGGTTCGGC	GCCGAACCGGCCcgcGATGCCGCCCTC
eisR128A(NHis) (pET28a)	CGGCATCTACGGCgcgTTCGGCTACGGGC	GCCCGTAGCCGAAcgcGCCGTAGATGCCG
eisR148A(NHis) (pET28a)	CCGACGCTTCGCGgcgTTTCACGCCGACG	CGTCGGCGTGAAAcgcCGCGAAGCGTCGG
eisW197A(NHis) (pET28a)	CCGCAGGTGCTCgcgGACGAGCTGCTG	CAGCAGCTCGTCcgcGAGCACCTGCGG
eisD292A(NHis) (pET28a)	ACCTGGCGCCAGgcgGGCCTGTGGTTG	CAACCACAGGCCcgcCTGGCGCCAGGT
eisY310A(NHis) (pET28a)	GAGGCGCGTGGTgcgGCTCACGAAGTT	AACTTCGTGAGCcgcACCACGCGCCTC

The introduced restriction sites are underlined for each primer. The 5' primers all introduced an *Nde*I restriction site. The 3' primer for *eis*(NHis) (pET28a) and all *eis* mutants introduced a *Bam*HI restriction site, whereas the 3' primer for *eis*(CHis) (pET22b) introduced a *Hind*III restriction site. The mutation site is indicated in lower-case.

The tags added to the Eis proteins are:

NHis (pET28a/*Nde*I) = MGSSHHHHHHSSGLVPRGSHMLQSDS

CHis (pET22b/*Hind*III) = KLAALEHHHHHH

3.2. Overproduction and purification of Eis proteins and mutants

All overexpression constructs were transformed into *E. coli* BL21 (DE3) chemically competent cells prior to expression and stored as frozen Luria-Bertani (LB)/glycerol stocks at -80 °C. 1 L of LB medium supplemented with appropriate antibiotics (KAN (50 μg/mL) for the pET28a constructs or ampicillin (100 μg/mL) for the pET22b construct) was inoculated with 10 mL of overnight cultures of each transformant and grown at (37 °C, 200 rpm) to attenuance of ~0.6 at 600 nm before induction with IPTG (final concentration of 500 μM). The induced cultures were grown for an additional 6 h (28 °C (all full length Eis and deletion mutants, and F24A, F84A, Y126A, W197A, D292A), 200 rpm) or overnight (15 °C (S121A) or 20 °C (F27A, I28A, W36A, V87A, R93A, H119A, R128A, R148A, and Y310A), 200 rpm) after which the cells were harvested by centrifugation (6000 rpm, 10 min, 4 °C, Beckman Coulter Aventi JE centrifuge, F10 rotor). The cell pellets were resuspended in lysis buffer [300 mM NaCl, 50 mM Na_2HPO_4 pH 8.0, adjusted at room temperature (rt), 10% glycerol] and lysed (1 pass at 10,000-15,000 psi through an Avestin EmulsiFlex-C3 high-pressure homogenizer). The insoluble cell debris were removed by centrifugation (16,000 rpm, 45 min, 4 °C, Beckman Beckman Coulter Aventi JE centrifuge, JA-17 rotor). Imidazole (final concentration of 2 mM) was added to the clear supernatant and incubated with 2 mL of Ni-NTA agarose resin (Qiagen) (for 2 h with gentle rocking at 4 °C). The resin was loaded onto a column and washed with 10 mL of lysis buffer containing 5 mM imidazole. The protein was then eluted with lysis buffer in a stepwise imidazole gradient (10 mL fraction of 20 mM (1x), 5 mL fractions of 20 mM (2x), 40 mM (3x), and 250 mM imidazole (3x)). The eluted fractions containing more than 95% pure desired proteins, as determined by SDS-PAGE, were pooled, dialyzed extensively against 50 mM Tris-HCl pH 8.0 at 4 °C, and concentrated using Amicon® Ultra PL-10 (10,000 MWCO). For structural studies, the proteins were further purified by S-200 size exclusion chromatography in the gel filtration buffer (50 mM Tris-HCl, pH 8.0 adjusted at rt, flow rate: 1.5 mL/min). Protein concentrations were determined using a Nanodrop spectrometer (Thermo Scientific). Protein yields (in mg/L of culture) were 0.94 (Eis(NHis)), 0.50 (Eis(CHis)), 0.17 (1-311), 0.50 (1-399), 0.21 (292-402), 0.87 (F24A), 0.58 (F27A), 0.66 (I28A), 0.31 (W36A), 0.22 (F84A), 0.31 (V87A), 0.38 (R93A), 0.52 (H119A), 0.45 (S121A), 1.28 (Y126A), 0.52 (R128A), 0.48 (R148A), 0.12 (W197A), 0.28 (D292A), and 0.07 (Y310A) (Fig. S3). All proteins were stored at 4 °C and found to be stable under these storage conditions for at least 2 months.

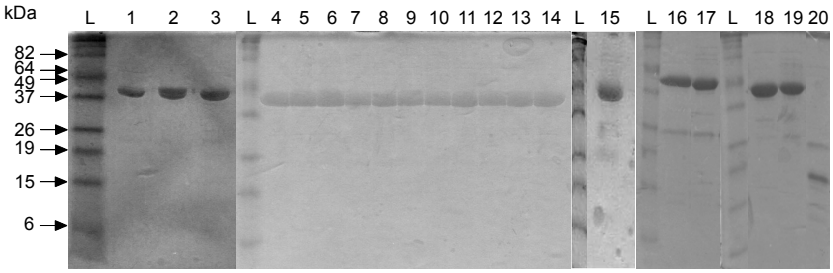

Fig. S3. Coomasie blue-stained 15% Tris-HCl SDS-PAGE gel showing the purified Eis proteins: wild-type (46597 Da, lane 1), SeMet (47019 Da, lane2), 1-399 (46173 Da, lane 3), Y310A (46505 Da, lane 4), F84A (46521 Da, lane 5), F24A (46521 Da, lane 6), W36A (46482 Da, lane 7), H119A (46530 Da, lane 8), R128A (46512 Da, lane 9), R93A (46512 Da, lane 10), R148A (46512 Da, lane 11), V87A (46569 Da, lane 12), I28A (46555 Da, lane 13), F27A (46521 Da, lane 14), wild-type (CHis) (45483 Da, lane 15), W197A (46405 Da, lane 16), D292A (46553 Da, lane 17), S121A (46581 Da, lane 18), Y126A (46505 Da, lane 19), and 292-402 (14317 Da, lane 20). L indicates the BenchMark™ pre-stained protein ladder from Invitrogen. 6 μg of each protein were loaded on the gel after boiling the protein samples in loading dye for 5 min.

3.3. Expression and purification of SeMet-Eis

Ten colonies of the fresh transformant harboring the pEis-pET28a(NHis) construct were inoculated into 6 mL of LB medium supplemented with KAN (50 μg/mL). The culture was grown at 37 °C to an attenuance of 0.34 at 600 nm. This LB culture (100 μL) was then used to inoculate 20 mL of minimal media (MM) (1× M9 salts, 0.4% glucose (10% stock), 1 μg/mL thiamine (10 mg/mL stock), 0.1 mM $CaCl_2$ (500 mM stock), and 2 mM $MgSO_4$ (1 M stock), supplemented with KAN (50 μg/mL)). The culture was grown (200 rpm, 37 °C) to an attenuance of 0.3 at 600 nm. This 20 mL culture was then used to inoculate 200 mL of MM, and the cells were grown (200 rpm, 37 °C) to attenuance of 0.3 at 600 nm. Subsequently, this 200 mL culture was utilized to inoculate 1 L of MM, and the culture was grown (200 rpm, 37 °C) to an attenuance of 0.4 at 600 nm. At this moment, L-leucine (50 mg/L), L-isoleucine (50 mg/L), L-valine (50 mg/L), L-lysine (100 mg/L), L-threonine (100 mg/L), L-phenylalanine (100 mg/L), and L-SeMet (75 mg/L) were added. All amino acids were prepared by dissolving into 5 mL of distilled H_2O, except for L-phenylalanine, for which 5 μL of 10 M NaOH was added to the solution. The 1 L culture was incubated (200 rpm, 37 °C) for an additional 33 min before induction with IPTG (final concentration, 500 μM). The induced culture was grown (200 rpm, 28 °C) for an additional 8 h. The cells were harvested by centrifugation (6000 rpm, 10 min, 4 °C). The cell lysis and Ni^{2+}-chelating chromatography steps were carried out as described above. β-mercaptoethanol (0.7 μL) was added to each fraction (5 mL) to prevent oxidation of the SeMet protein. Fractions containing the desired protein [as determined by SDS-PAGE] were combined

and further purified by FPLC (1.5 mL/min using 50 mM Tris-HCl, pH 8.0 adjusted at rt, 2 mM β-mercaptoethanol) (Fig. S4). The pure protein was concentrated using Amicon® Ultra PL-10 (10,000 MWCO). Protein concentration was determined using a Nanodrop spectrometer (Thermo Scientific). SeMet-Eis used for crystallization was concentrated to 4.74 mg/mL and stored at 4 °C. The yield of SeMet-Eis was 0.53 mg/L of culture.

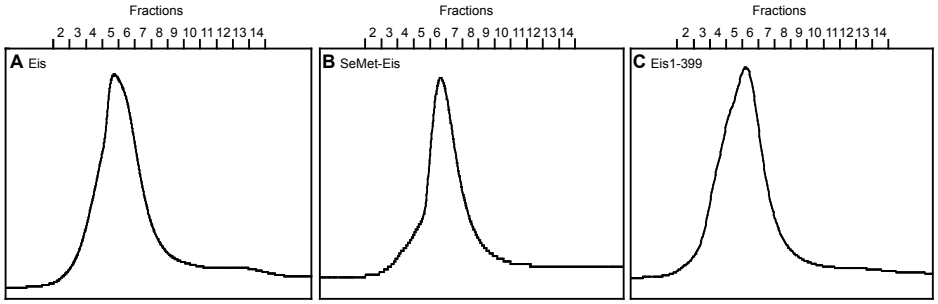

Fig. S4. Size-exclusion chromatogram of **A.** Eis, **B.** SeMet-Eis, and **C.** Eis1-399. Panel **C** shows that the C-terminal portion of the Eis tail (amino acid residues 400-402) is not required for hexamerization of Eis.

4. Biochemical characterization of Eis proteins and mutants

4.1. Determination of AG profile for all Eis proteins and mutants by UV-Vis assay

The acetyltransferase activity of Eis proteins was monitored by a UV-Vis assay in which the free thiol group of CoA, generated by enzyme catalyzed reaction, is coupled to 4,4'-dithiodipyridine (DTDP) to produce thiopyridone, which can be monitored by increase in absorbance at 324 nm (ε_{324} = 19 800 $M^{-1}cm^{-1}$) (2). The reaction mixtures (100 μL) containing AcCoA (0.5 mM, 5 eq), AG (0.1 mM, 1 eq), DTDP (2 mM), and Tris-HCl pH 8.0 (50 mM), were initiated by adding protein (0.5 μM) at 25 °C. Reactions were monitored by taking readings every 30 s for 15 min in 96-well plate format. Using this assay, APR, SPT, and STR were found to not be substrates of Eis(NHis), whereas AMK, HYG, KAN, NEA, NEO, NET, PAR, RIB, SIS, and TOB were found to be substrates of this enzyme. Therefore, only the last ten AGs were tested with Eis(CHis) and Eis deletion and single point mutants (Figs. S5 and 4 in main text).

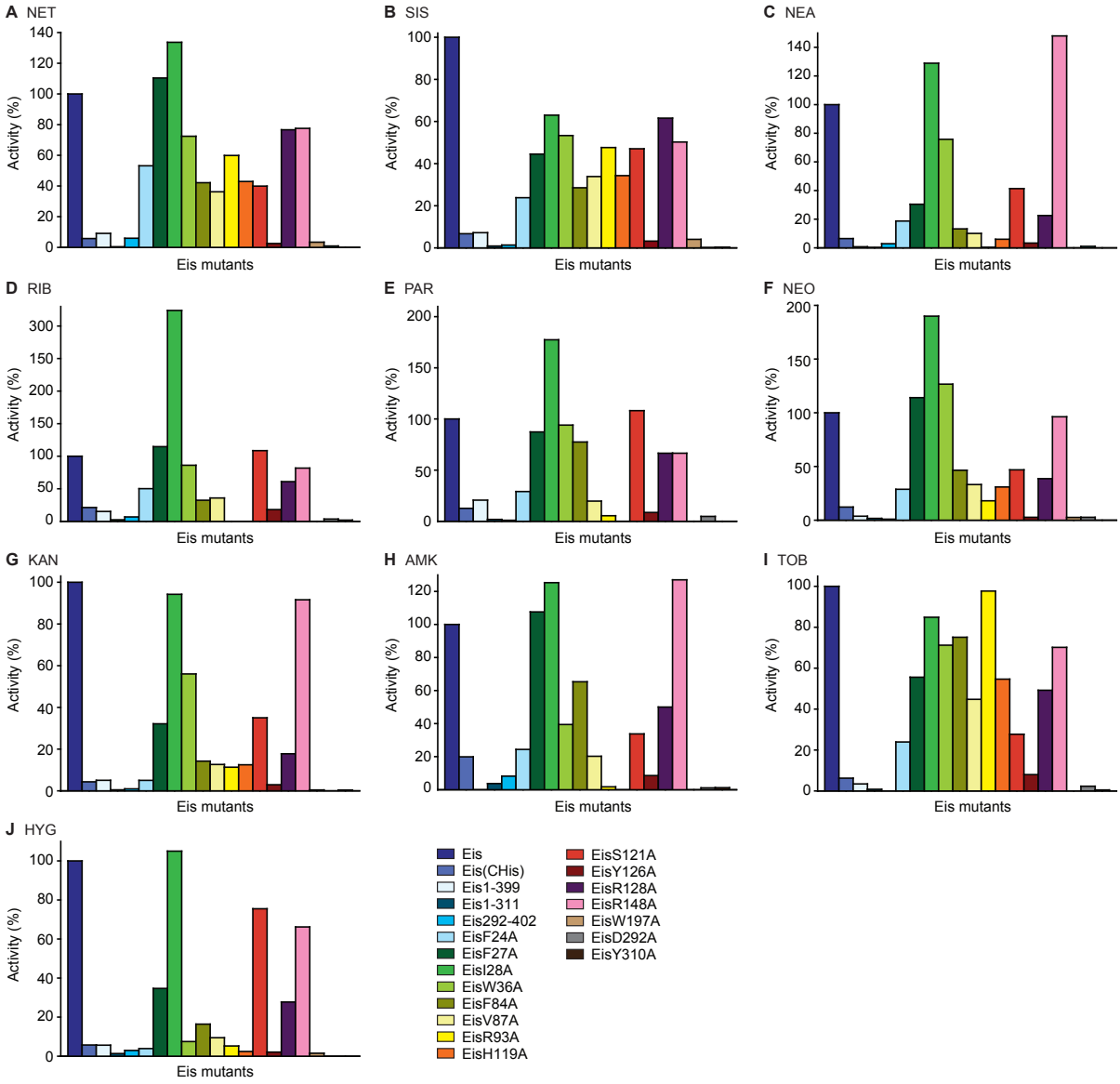

Fig. S5. Relative activity towards the ten AGs tested for all Eis proteins and mutants studied. All activities are calculated relative to the activity of the wild-type Eis with the respective AGs.

4.2. Determination of number of sites acetylated on each AG by all Eis proteins and mutants by UV-Vis assay and LCMS

As described above, reaction mixtures (100 μL) containing AG (0.1 mM), DTDP (2 mM), Tris-HCl (50 mM, pH 8.0 adjusted at rt), and AcCoA (0.1 mM, 1 eq or 0.5 mM, 5 eq), were initiated by adding protein (0.5 μM) at 25 °C. Reactions were monitored at 324 nm by taking readings every 30 s until reaching plateau (Fig. 1 in main text). To confirm the established number of acetylation sites for each AG substrate by each Eis proteins/mutants, reactions (30 μL)

containing AG (0.67 mM, 1 eq), AcCoA (6.7 mM, 10 eq), Tris-HCl (50 mM, pH 8.0 adjusted at rt), and Eis proteins/mutants (10 μM) were performed overnight at 25 °C. Ice-cold MeOH (30 μL) was added to the reaction mixture, which was then kept at -20 °C for at least 20 min. The precipitated protein was removed by centrifugation (13,000 rpm, rt, 10 min). The masses of the novel acetylated AGs present in each sample were determined by LCMS in positive mode using H_2O (0.1% formic acid) after dilution of the supernatant (10 μL) with H_2O (20 μL) and injection of all 30 μL (Table S2). Representative MS of all AGs modified by Eis are provided in Fig. S6.

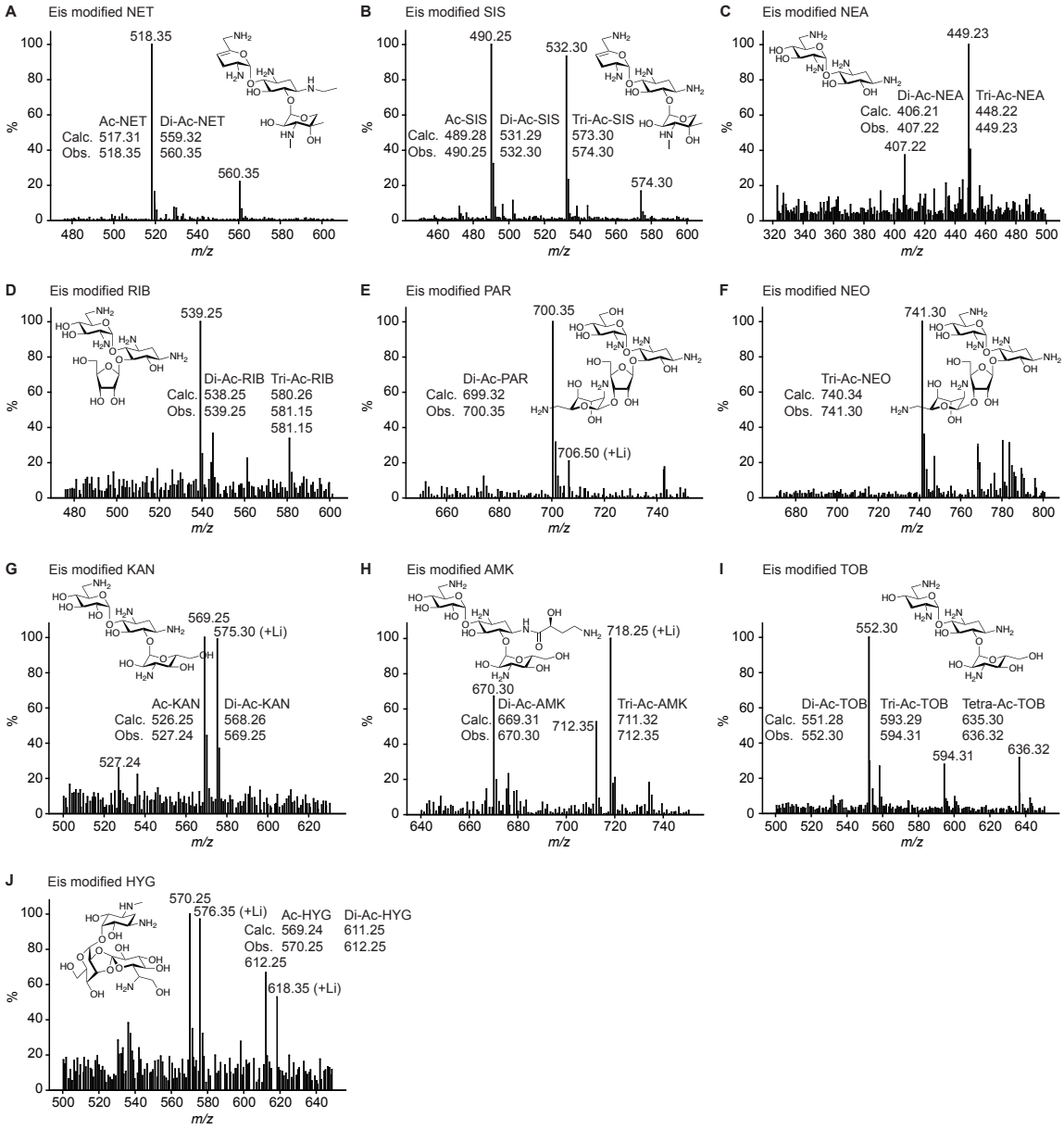

Fig. S6. Representative mass spectra of AGs multi-acetylated by Eis.

Table S2. Mass analysis of aminoglycosides (AGs) acetylated by the Eis protein and its mutants.

	Calculated	$[M + H]^+$	Observed[f] $[M + H]^+$							
AG[a]			(NHis)	(CHis)	1-399	F24A	F27A	I28A	W36A	F84A
AMK	Mono[b]	628.30					628.25			
	Di[c]	670.31	670.30				670.20			
	Tri[d]	712.32	712.35							
HYG	Mono	570.24	570.25				570.20	570.25		
	Di	612.25	612.25							
KAN	Mono	527.25	527.24						527.25	
	Di	569.26	569.25				569.25	569.20		
NEA	Mono	365.20								
	Di	407.21	407.22				407.15	407.20	407.22	
	Tri	449.22	449.23							
NEO	Mono	657.32								657.32
	Di	699.33					699.35	699.35	699.25	
	Tri	741.34	741.30			741.30	741.35	741.35	741.40	
NET	Mono	518.31	518.35	518.35	518.25	518.35	518.25	518.20	518.35	518.35
	Di	560.32	560.35	560.35	560.35	560.35	560.25	560.30		560.35
PAR	Mono	658.31					658.25			658.31
	Di	700.32	700.35				700.25		700.40	700.35
	Tri	742.33								
RIB	Mono	497.24								
	Di	539.25	539.25				539.25	539.35		
	Tri	581.26	581.15							
SIS	Mono	490.28	490.25	490.25	490.30	490.25	490.30	490.25	490.30	490.25
	Di	532.29	532.30	532.30	532.30	532.25	532.30	532.30		532.30
	Tri	574.30	574.30							
TOB	Mono	510.27				510.28				510.27
	Di	552.28	552.30			552.30	552.20	552.25	552.30	552.30
	Tri	594.29	594.31							
	Tetra[e]	636.30	636.32							

	Calculated	$[M + H]^+$	Observed[f] $[M + H]^+$							
AG[a]			V87A	R93A	H119A	S121A	R128A	R148A	W197A	D292A
AMK	Mono	628.30						628.25		
	Di	670.31						670.20		
	Tri	712.32								
HYG	Mono	570.24				570.25		570.35		
	Di	612.25								
KAN	Mono	527.25				527.24				
	Di	569.26				569.25		569.30		
NEA	Mono	365.20								
	Di	407.21				407.23				
	Tri	449.22				449.23		449.22		
NEO	Mono	657.32			657.30	657.32				
	Di	699.33	699.35		699.30		699.35			
	Tri	741.34						741.35		
NET	Mono	518.31	518.35	518.25	518.25	518.35	518.35		518.35	518.30
	Di	560.32		560.20		560.35	560.20	560.25	560.30	560.30
PAR	Mono	658.31				680.31 (+Na)	658.25	658.25		
	Di	700.32				700.35				
	Tri	742.33				742.34				
RIB	Mono	497.24								
	Di	539.25								
	Tri	581.26								
SIS	Mono	490.28	490.30		490.25	490.25			490.25	490.20
	Di	532.29	532.30			532.32	532.25	532.20	532.25	532.35
	Tri	574.30				574.30	574.30			
TOB	Mono	510.27	510.28							
	Di	552.28	552.25	552.30	552.30	552.30	552.30	552.30		
	Tri	594.29			594.20	594.31				
	Tetra	636.30				636.32				

[a]APR, SPT, and STR were found not to be substrates of Eis. [b]Mono indicates mono-acetylation. [c]Di indicates di-acetylation. [d]Tri indicates tri-acetylation. [e]Tetra indicates tetra-acetylation. [f]Note: The deletion mutants Eis1-311 and Eis292-402 as well as the single point mutants EisY126A and Y310A did not exhibit any activity.

To confirm the uniqueness of multi-acetylation by Eis, we tested with 10 eq of AcCoA and all 10 AG substrates of Eis the six following AACs: AAC(2')-Ic from *Mtb* (2, 3), AAC(3)-IV from *Escherichia coli* (4, 5), AAC(3)-Ib and AAC(6')-Ib' from the bifunctional AAC(3)-Ib/AAC(6')-Ib' from *Pseudomonas aeruginosa* (6, 7), AAC(6') from the bifunctional AAC(6')/APH(2")-Ia

from *Staphylococcus aureus* (4, 8), and AAC(6')-IId from the bifunctional ANT(3")-Ii/AAC(6')-IId from *Serratia marcescens* (9, 10). We found each of them to only mono-acetylate all AGs tested.

4.3. Steady-state kinetic measurements of net acetylation of AGs by Eis

Table S3. Kinetic parameters of net acetylation by Eis.

AG	K_m (μM)	k_{cat} (s^{-1})	k_{cat}/K_m ($M^{-1}s^{-1}$)
AMK	75 ± 3	0.020 ± 0.007	267
KAN	99 ± 5	0.039 ± 0.004	394
NEA	178 ± 2	0.070 ± 0.002	393
NEO	98 ± 8	0.130 ± 0.019	1,327
NET	48 ± 5	0.482 ± 0.037	10,042
PAR	82 ± 9	0.058 ± 0.009	707
SIS	58 ± 15	0.270 ± 0.024	4,655
TOB	63 ± 6	0.162 ± 0.004	2,571

The kinetic parameters for Eis acetylation of several AGs (AMK, KAN, NEA, NEO, NET, PAR, SIS, and TOB) were determined at 25 °C in reactions (100 μL) containing a fixed concentration of AcCoA (0.1 mM), varied concentrations of AGs (0, 20, 50, 100, 250, 500 μM), DTDP (2 mM), Tris-HCl pH 8.0 (50 mM), and Eis (0.25 μM). Reactions were initiated by the addition of AcCoA and were carried out in duplicate. Net acetylation was monitored by measuring absorbance at 324 nm (as described in Section 4.1) as a function of time. The kinetic parameters, K_m and k_{cat} (Table S3) were determined from the linear parts of these time courses by using Lineweaver-Burk plots.

4.4. Determination of amine positions acetylated by Eis

In order to establish the amine positions acetylated by Eis, NEA was chosen as the model AG. Control experiments with other AG acetyltransferases (AAC(2')-Ic, AAC(3)-IV, and AAC(6')) known and confirmed by us by UV-Vis assays and LCMS to acetylate only at the 2'-, 3, and 6'-positions, respectively (whenever available) of all AG substrates used in this study were performed.

4.4.1. Preparation of pAAC(2')-Ic-pET28a(NHis) overexpression construct

The gene encoding AAC(2')-Ic was PCR-amplified using *M. tuberculosis* H37Rv genomic DNA and Phusion DNA polymerase as described by NEB. The forward and reverse primers used were 5'-ATTCCATATGCACACCCAGGTACACACGG-3' and 5'-GCGGAATTCTTACCAGACGTCGCCCGC-3', respectively (the *Nde*I and *Eco*RI restriction sites are underlined). The amplified gene was inserted into the linearized pET28a vector via the corresponding *Nde*I/*Eco*RI restriction sites. Expression of AAC(2')-Ic-pET28a was done following transformation into *E. coli* TOP10 competent cells. The expression clone was characterized by DNA sequencing (The University of Michigan DNA Sequencing Core) and

compared to its corresponding gene sequence from *M. tuberculosis* (GenBank accession no. U72714).

4.4.2. Overproduction and purification of AAC(2')-Ic, AAC(3)-IV, and AAC(6')/APH(2")

The AAC(3)-IV and AAC(6')/APH(2") proteins were overexpressed and purified as previously described (4). As none of the reactions performed in this study contain a nucleotide substrate for the APH(2") domain of the bifunctional AAC(6')/APH(2") protein, for the sake of simplicity we will call this bifunctional enzyme AAC(6') in the text. For the production of AAC(2')-Ic, the protocol described for the purification of Eis protein was used with the following modifications: The cells were grown at 37 °C to attenuance of ~1.0 at 600 nm prior to cooling to 20 °C for 15 min before induction with IPTG (200 μM final concentration) and additional growth at 20 °C for 9 h. The lysis buffer utilized was composed of 25 mM triethanolamine pH 7.8 adjusted at rt, 50 mM NaCl, 1 mM EDTA, and 10% (v/v) glycerol. The dialysis buffer contained the same components as the lysis buffer with additional 1 mM DTT and 1 mM EDTA. Glycerol (50% final concentration) was added to the pure AAC(2')-Ic protein after dialysis and concentration. 0.3 mg of AAC(2')-Ic was obtain per L of culture (Fig. S7). The protein was stored at -20 °C.

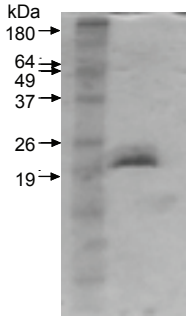

Fig. S7. Coomassie blue-stained 15% Tris-HCl SDS-PAGE gel showing the purified AAC(2')-Ic (22332 Da). 6 μg of protein were loaded on the gel.

4.4.3. TLC assays

The eluent system utilized for all TLCs of reactions performed with NEA was 3:0.8/MeOH:NH_4OH. The R_f values observed are reported in Table S4. The exact reaction conditions are reported below. TLCs showing the various mono-, di-, and tri-acetylated NEA are presented in Fig. 2 in main text.

4.4.3.1. Control TLCs of AGs mono-acetylated at the 2'-, 3-, and 6'-position by AAC(2')-Ic, AAC(3)-IV, and AAC(6'), respectively

Reactions (15 μL) were carried out at rt in MES buffer (50 mM, pH 6.6 adjusted at rt) (AAC(3)-IV and AAC(6')) or in potassium phosphate buffer (100 mM, pH 7.0 adjusted at rt) (AAC(2')-Ic) in the presence of acetyl-CoA (0.96 mM, 1.2 eq), AG (0.8 mM, 1 eq), and AAC enzyme (10 μM). After overnight incubation, aliquots (5 μL) of the reaction mixtures were loaded and run onto a TLC plate.

4.4.3.2. Control TLCs of AGs di-acetylated sequentially by pairwise treatment with AAC(2')-Ic, AAC(3)-IV, and AAC(6')

Reactions (10 μL) were carried out at rt in MES buffer (50 mM, pH 6.6 adjusted at rt) in the presence of acetyl-CoA (1.92 mM, 2.4 eq), AG (0.8 mM, 1 eq), and AAC enzyme (10 μM). After overnight incubation, the second AAC enzyme (10 μM) was added to the reaction mixture, which was incubated for an additional 16 h. Aliquots (5 μL) of each di-acetylation reaction mixture were loaded and run onto a TLC plate.

4.4.3.3. TLCs showing time course of tri-acetylation of NEA by Eis

Reactions (30 μL) were carried out at rt in Tris-HCl buffer (50 mM, pH 8.0 adjusted at rt) in the presence of acetyl-CoA (4 mM, 5 eq), NEA (0.8 mM, 1 eq), and Eis (5 μM). Aliquots (4 μL) were loaded and run onto a TLC plate after 0, 5, 10, 30, and 120 min as well as after overnight incubation (Table S4 and Fig. 2 in main text).

Table S4. R_f values[a] of mono-, di-, and tri-acetylated NEA by the AAC(2')-Ic, AAC(3)-IV, AAC(6'), and Eis proteins.

		Enzymes utilized											
		None	(2')[f]	(3)[g]	(6')[h]	(3) then (2')	(6') then (2')	(6') then (3)	Eis				
AG									5 min	10 min	30 min	2 h	O/N
NEA	Parent	0.11							0.11	0.11			
	Mono		0.14	0.18	0.22				0.14	0.14	0.14	0.14	
	Di					0.35	0.27	0.37	0.27	0.27	0.27	0.27	
	Tri[e]											0.39	0.39

[a]The eluent system used for TLCs was 3:0.8/MeOH:NH_4OH. [b]Parent indicates non-acylated. [c]Mono indicates mono-acetylation. [d]Di indicates di-acetylation. [e]Tri indicates tri-acetylation. [f](2') indicates AAC(2')-Ic. [g](3) indicates AAC(3)-IV. [h](6') indicates AAC(6') of the AAC(6')/APH(2").

4.4.4. Triacetylation of NEA by Eis and NMR analysis of the 1,2',6'-triacetyl-NEA product

In order to establish which 3 positions Eis acetylates on NEA, a large-scale reaction was performed. Briefly, a reaction mixture (5 mL) containing NEA (5 mM, 1 eq), acetyl-CoA (25 mM, 5 eq), and Eis (0.5 mg) in Tris-HCl (50 mM, pH 8.0 adjusted at rt) was incubated with

gentle shaking at rt for 48 h prior to addition of additional portions of acetyl-CoA (5 mM) and Eis (0.1 mg) followed by further incubation for 24 h. The progress of the Eis reaction was monitored by LCMS. After 90% conversion of NEA into triacetyl-NEA, the Eis enzyme was removed from the mixture by filtration using an Amicon® Ultra-4 centrifugal filter (3000 MWCO), and the filtrate was lyophilized prior to further purification. The lyophilized solid was dissolved in H_2O (5 mL) and purified by flash chromatography (SiO_2; 1:1/MeOH:H_2O, R_f 0.39 (3:0.8/MeOH:NH_4OH)) to give 1,2',6'-triacetyl-NEA as a white powder after removal of the solvents by concentration under reduced pressure followed by lyophilization. For NMR analyses, 1,2',6'-triacetyl-NEA was dissolved in D_2O (3 mL) and the pH was adjusted to ~3.0 by addition of H_2SO_4 (5%) prior to lyophilization and further re-dissolving in D_2O or 9:1/H_2O:D_2O. The positions of acetylation, purity, and structure identification were confirmed by ^1H, ^{13}C, 2D-TOCSY, 2D-COSY, DEPT, and HETCOR NMR as well as LCMS. Proton connectivities were assigned using 2D-TOCSY and 2D-COSY spectra. Signals of all carbons were derived by examination of HETCOR and DEPT spectra. Representative spectra for 1,2',6'-triacetyl-NEA are provided in Figs. S9, S11, and S12.

To unambiguously establish the 3 acetylated positions on the NEA scaffold, the ^1H and ^{13}C NMR were compared to a standard of pure non-acetylated NEA (Tables S5-6). The sample of NEA for NMR was prepared as described for the 1,2',6'-triacetyl-NEA NMR sample. Representative spectra for NEA are provided in Figs. S8 and S10.

Table S5. Proton chemical shifts determined for NEA and 1,2',6'-triacetyl-NEA.[a]

Ring	H position	NEA[d]	1,2',6'-triacetyl-NEA	Δppm
II	1	3.41-3.36 (m)[b] [3.38][c]	3.89-3.74 (m) [3.84]	**0.46**
	2_{ax}	2.04 (ddd (app. q), $J_{2ax,2eq} = J_{2ax,1} = J_{2ax,3}$ = 12.6 Hz)	1.68 (ddd (app. q), $J_{2ax,2eq} = J_{2ax,1} = J_{2ax,3}$ = 12.8 Hz)	-0.36
	2_{eq}	2.55 (ddd (app. dt), $J_{2eq,2ax}$ = 12.6 Hz, $J_{2eq,1} = J_{2eq,3}$ = 4.1 Hz)	2.32 (ddd (app. dt), $J_{2eq,2ax}$ = 12.8 Hz, $J_{2eq,1} = J_{2eq,3}$ = 4.2 Hz)	-0.23
	3	3.59 (ddd, $J_{3,2ax}$ = 12.6 Hz, $J_{3,4}$ = 10.3 Hz, $J_{3,2eq}$ = 4.1 Hz)	3.51-3.43 (m) [3.50]	-0.09
	4	4.10-4.04 (m) [4.10]	3.89-3.74 (m) [3.73]	-0.37
	5	3.75 (t, J = 9.1 Hz)	3.69-3.64 (m) [3.66]	-0.09
	6	3.66 (t, J = 9.9 Hz)	3.51-3.43 (m) [3.47]	-0.19
I	1'	6.04 (d, $J_{1',2'}$ = 3.9 Hz)	5.48 (d, $J_{1',2'}$ = 3.9 Hz)	-0.56
	2'	3.51-3.48 (m) [3.49]	4.01 (dd, $J_{2',3'}$ = 10.8 Hz, $J_{2',1'}$ = 3.9 Hz)	**0.52**
	3'	4.10-4.04 (m) [4.07]	3.89-3.74 (m) [3.80]	-0.27
	4'	3.51-3.48 (m) [3.50]	3.51-3.43 (m) [3.44]	-0.06
	5'	4.10-4.04 (m) [4.05]	3.89-3.74 (m) [3.82]	-0.23
	$6'_a$	3.27 (dd, $J_{6'a,6'b}$ = 13.5 Hz, $J_{6'a,5'}$ = 8.0 Hz)	3.55 (dd, $J_{6'a,6'b}$ = 14.6 Hz, $J_{6'a,5'}$ = 3.4 Hz)	**0.28**
	$6'_b$	3.54 (dd, $J_{6'b,6'a}$ = 13.5 Hz, $J_{6'b,5'}$ = 3.2 Hz)	3.69-3.64 (m) [3.65]	**0.11**
Acetyl	N<u>H</u>-1	×	8.20 (d, $J_{NH,1}$ = 3.7 Hz)*	
	N<u>H</u>-2'	×	8.21 (d, $J_{NH,2'}$ = 4.6 Hz)*	
	N<u>H</u>-6'	×	8.12 (t, $J_{NH,6'}$ = 5.8 Hz)*	
	C<u>H</u>$_3$C=O	×	2.08 (s)	
	C<u>H</u>$_3$C=O	×	2.07 (s)	
	C<u>H</u>$_3$C=O	×	2.05 (s)	

[a]The chemical shift were established based on ^{1}H, 2D-TOCSY and 2D-COSY NMR. [b]Multiplicity and J are given in (). [c]The numbers in [] were determined from 2D-COSY. [d]The chemical shifts reported for NEA are in accordance with those previously reported in the literature (11, 12). *Indicates that the values were determined from spectra taken in 9:1/H_2O:D_2O. ×Indicates that acetyl moiety is not present in the molecule.

Table S6. Carbon chemical shifts determined for NEA and 1,2',6'-triacetyl-NEA.[a]

Ring	C position	NEA[b]	1,2',6'-triacetyl-NEA	Δppm
II	1	49.7	48.8	**-0.9**
	2	28.1	30.2	2.1
	3	48.4	49.7	1.3
	4	76.7	79.8	3.1
	5	75.2	75.7	0.5
	6	72.4	74.1	1.7
I	1'	95.3	98.2	2.9
	2'	53.5	53.3	**-0.2**
	3'	68.1	69.9	1.8
	4'	71.0	71.3	0.3
	5'	69.1	70.7	1.6
	6'	40.4	39.5	**-0.9**
Acetyl	CH$_3$<u>C</u>=O	×	174.9	
	CH$_3$<u>C</u>=O	×	174.5	
	CH$_3$<u>C</u>=O	×	174.2	
	<u>C</u>H$_3$C=O	×	22.0	
	<u>C</u>H$_3$C=O	×	21.9	
	<u>C</u>H$_3$C=O	×	21.8	

[a]The chemical shift were established based on ^{13}C, DEPT and HETCOR NMR. [b]The chemical shifts reported for NEA are in accordance with those previously reported in the literature (11, 12). ×Indicates that the acetyl moiety is not present in the molecule.

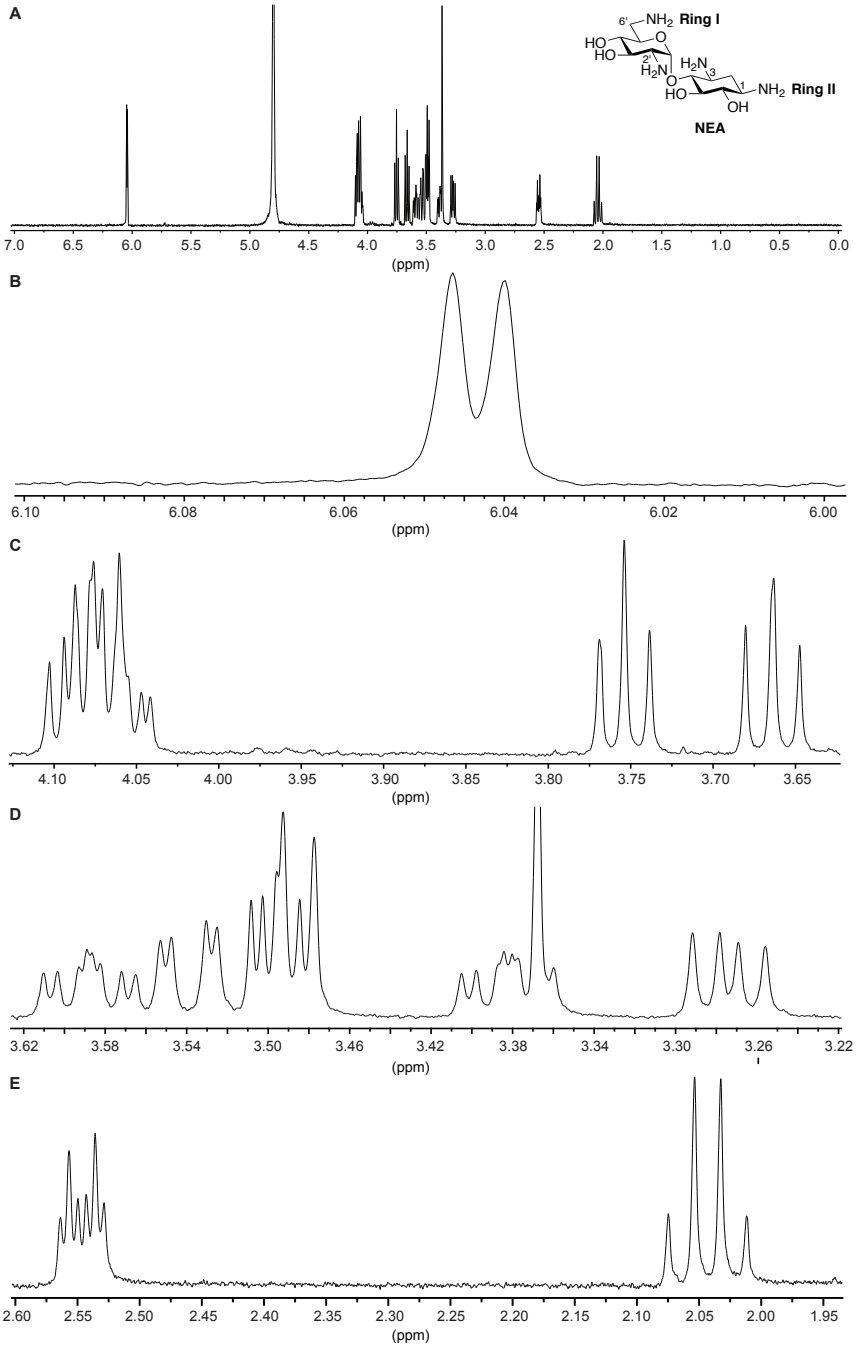

Fig. S8. ^{1}H NMR of NEA in D_2O. The full spectrum is shown in panel **A** and the expansions in panels **B-E**.

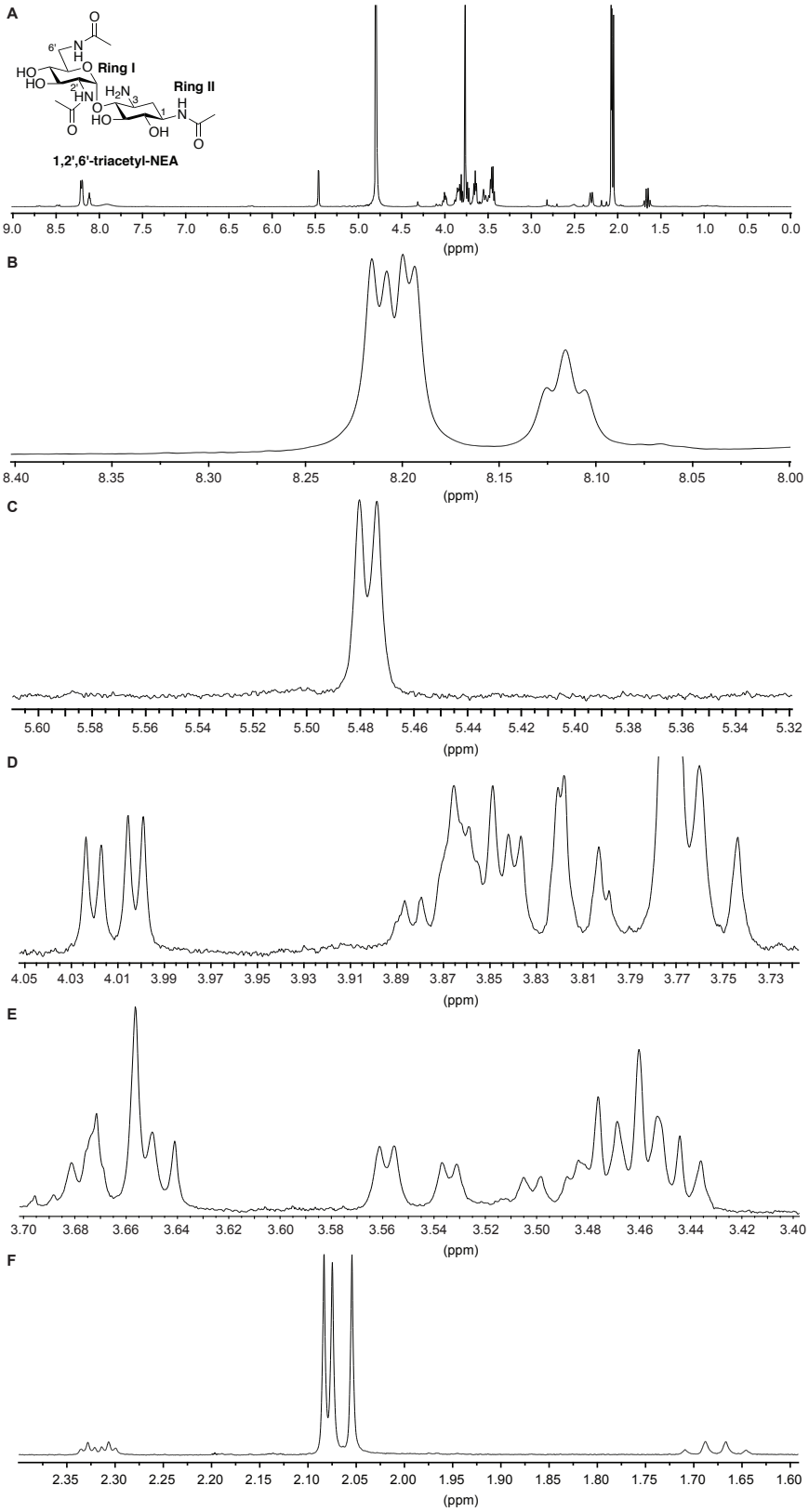

Fig. S9. ^{1}H NMR of 1,2',6'-triacetyl-NEA in 9:1/H_2O:D_2O (panels **A** and **B** to see the amide Hs) and in D_2O (panels **C**-**F**). The full spectrum is shown in panel **A** and the expansions in panels **B**-**F**.

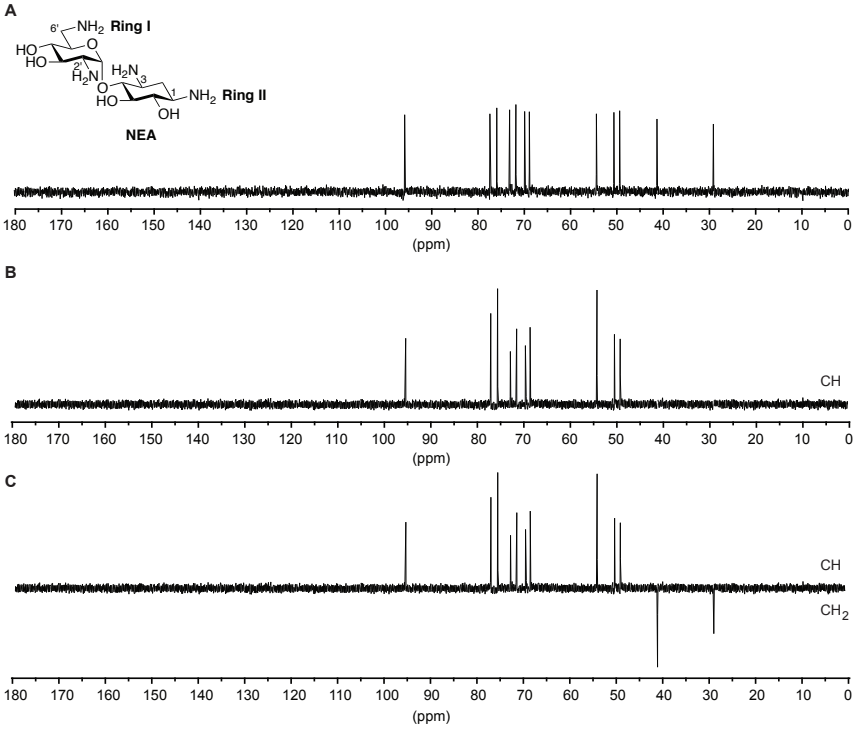

Fig. S10. ^{13}C DEPT of NEA in D_2O.

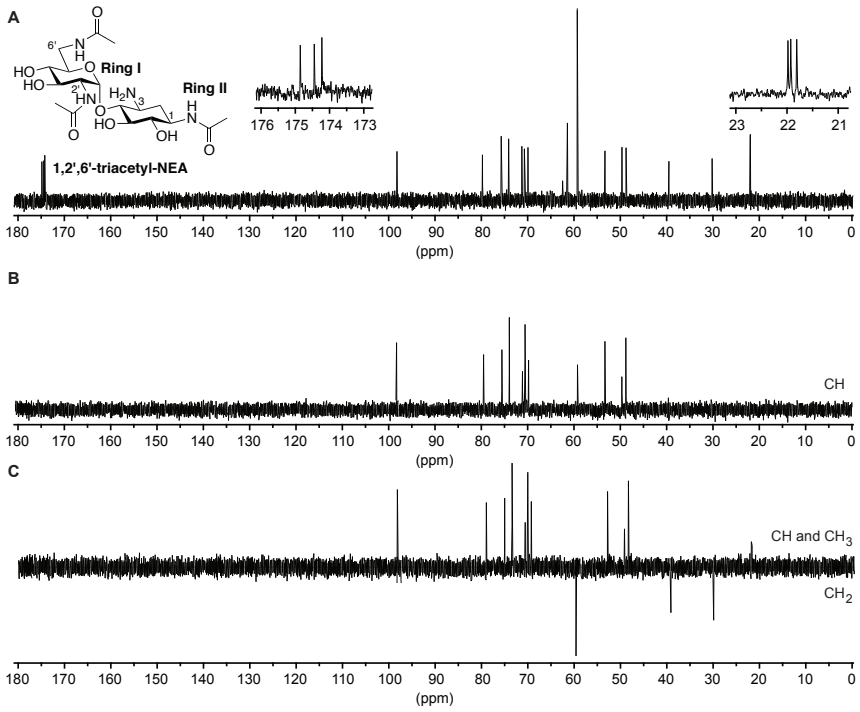

Fig. S11. ^{13}C DEPT of 1,2',6'-triacetyl-NEA in D_2O.

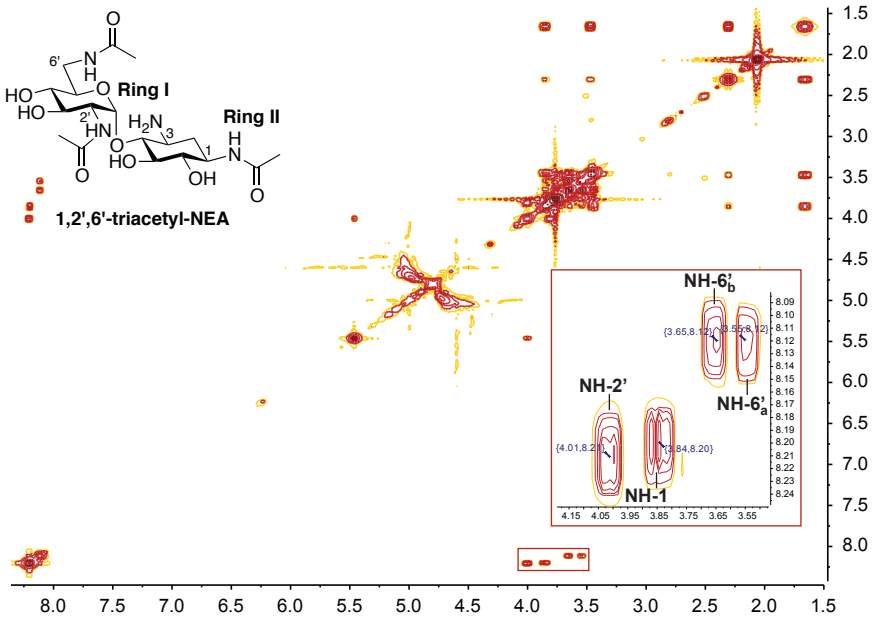

Fig. S12. 2D-COSY of 1,2',6'-triacetyl-NEA in 9:1/H_2O:D_2O. The insert shows the expansion for the amide protons connected to the protons at positions 1, 2', and 6' ($6'_a$ and $6'_b$ shown (note: a and b are arbitrarily assigned)).

5. Structural characterization of Eis

5.1. Crystallization, diffraction data collection, and structure determination and refinement of Eis

The initial conditions for growing SeMet-Eis-CoA co-crystals were found using Hampton Research Crystal Screen solutions (Hampton Research, Aliso Viejo, CA). Upon optimization, single crystals of SeMet-Eis-CoA (0.15 μm × 0.15 μm × 0.15 μm in size) were obtained in 2-3 weeks. Crystals were grown by hanging-drop vapor-diffusion technique at 22 °C. The drops contained 1 μL of a mixture of SeMet-Eis (3.5 mg/mL) in 50 mM Tris-HCl (pH 8.0, adjusted at rt), KAN (10 mM), and CoA (8.8 mM) mixed with 1 μL of the reservoir solution (Tris-HCl (pH 8.5, adjusted at rt) (0.1 M), PEG8000 (10-15% w/v), and $(NH_4)_2SO_4$ (0.1 or 0.4 M)) and were equilibrated against 1 mL of the reservoir solution. The crystals were gradually transferred into a cryoprotectant solution (Tris-HCl pH 8.5 (0.1 M), PEG8000 (10% w/v), $(NH_4)_2SO_4$ (0.1 M), glycerol (15%), and CoA (1 mM)) and flash-frozen in liquid nitrogen. The crystals of the native Eis-CoA-acetylated HYG ternary complex were grown and harvested analogously, but by using a different reservoir solution (Tris-HCl pH 8.5 (0.1 M) and PEG 8000 (8-12% w/v)), except that a mixture of Eis with CoA (1 mM) and KAN (10 mM) was used. The CoA and KAN molecules were soaked out of the crystals by a gradual replacement of the crystallization buffer with the

cryoprotectant solution (Tris-HCl pH 8.5 (0.1 M), PEG 8000 (8-12% w/v), and 15% glycerol) that contained AcCoA (1 mM) and 10 mM HYG (10 mM), and subsequent overnight incubation, before flash-freezing in the liquid nitrogen. Other AGs (KAN, NET, PAR, SIS, and AMK) were also tried in the growth and soaking of the crystals, with similar electron density in the active site. The best-diffracting crystals were obtained with the KAN (during growth) and HYG (during soak) pair.

Table S7. Crystallographic data collection and structure refinement statistics of Eis.

Data collection:		
	Native Eis in complex with CoA and acetylated HYG	***SeMet-Eis in complex with CoA, Se peak, wavelength = 0.9794 Å***
Space group	H32	P4$_1$22
Monomer per asymmetric unit	1	3
Unit cell dimensions		
a, b, c (Å)	174.9, 174.9, 124.7	109, 109, 142
α, β, γ (°)	90, 90, 120	90, 90, 90
Resolution (Å)	50.00-1.95 (1.98-1.95)[a]	50-2.7 (2.75-2.70)[a]
I/σ	19.8 (2.0)	28.4 (5.1)
Completeness (%)	96.8 (79.2)	99 (100)
Redundancy	5.4 (3.9)	12.4 (12.1)
R_{merge}	0.09 (0.47)	0.12 (0.73)
Number of unique reflections	100,857	59,864
Refinement:		
Resolution (Å)	40.00-1.95 (2.00-1.95)[a]	
R (%)	19.6 (24.8)	
R_{free} (%)	22.4 (34.2)	
Bond length deviation (rmsd) from ideal (Å)	0.013	
Bond angle deviation (rmsd) from ideal (°)	1.54	
Ramachandran plot statistics		
Residues in most favored and additional allowed regions (%)	100	
Residues in generously allowed regions (%)	0	
Residues in disallowed regions	0	

[a]Numbers in parentheses indicate the values in the highest resolution shell.

The diffraction data were collected at beamline 21-ID at the Advanced Photon Source at the Argonne National Laboratories. The data were indexed, integrated and scaled with HKL2000 (13). Initially, we attempted to determine the structure of the SeMet-Eis-CoA by molecular replacement using program PHASER (14) and a structure of a weakly homologous putative acetyltransferase from *Enterococcus faecalis* determined by the Midwest Center for Structural Genomics (PDB code: 2I00), as a search model. This approach yielded a clear solution, however the quality of the electron density map was not sufficiently high for refinement. By using sequence homology between this model and Eis, we obtained putative positions of 21 Se atoms (7 per monomer) in the asymmetric unit and used these heavy atom sites to obtain phases from the Se anomalous signal by the SAD phasing with PHASER (14). The resulting electron density map was of high quality and was readily interpretable. The structure of SeMet-Eis-CoA (KAN was not found in the difference density) was then built and refined iteratively using programs Coot (15) and REFMAC (16), respectively. This structure was used as a molecular replacement model to obtain the structure of Eis-CoA-acetylated HYG by PHASER. The Eis model was further altered and refined. The data collection and refinement statistics for the structures reported here are given in Table S7. In the omit electron density map

generated by using with Eis and no ligands or water, strong (>3.0σ) Fo-Fc density in the active site for bound CoA and the acetamide moiety of the acetylated HYG was present that allowed facile building and refinement of these ligands. The density for the rest of the HYG was too weak to allow us to build the rest of the AG molecule. Only the acetamide moiety of the acetylated AG was observed when other AGs were used in the crystal growth or soaking conditions. The Eis-CoA-acetamide structure was deposited in the Protein Data Bank with the PDB accession number 3R1K.

5.2. The structure of the Eis monomer

The topology of the assembly of the N-terminal (magenta, bottom panel) and the central (green, bottom panel) regions of Eis is presented in Fig. S13. The surface representation of the Eis monomer showing a complex and negatively charged substrate-binding cavity is depicted in Fig. S14.

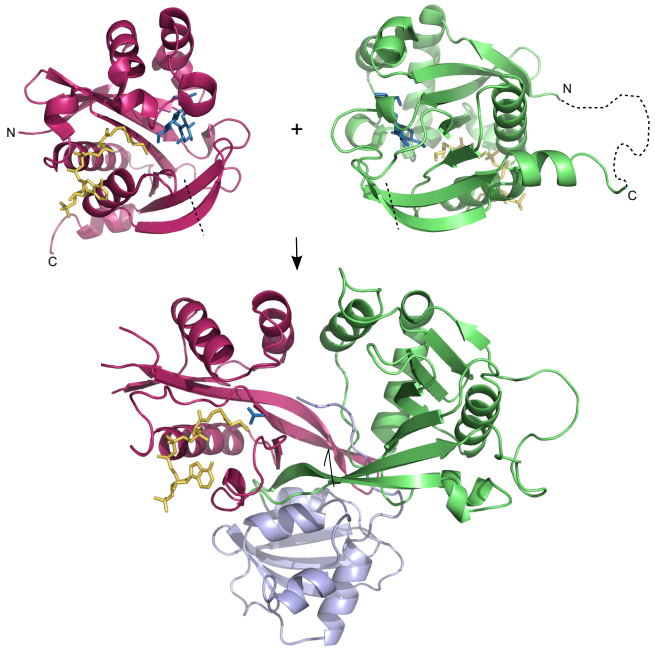

Fig. S13. Topology of the assembly of the N-terminal (magenta, bottom panel) and the central (green, bottom panel) GNAT regions of Eis. The N-terminal and the central regions have a GCN5-type fold. The structure of AAC(6')-Ib (PDB code: 2BUE) (17) that has a similar fold is shown in top left and right panels, each oriented and colored to match the respective regions of Eis below. The Eis fold topology can be obtained by breaking the two strands of the β-sheet in the two top structures and adjoining them as well as connecting the N- and the C-terminus of the top right fold (a cyclic permutation of a GNAT fold), as shown by the dashed lines. Therefore, Eis was likely a result of gene duplication and fusion events in which one of the two GNAT folds was cyclically permuted.

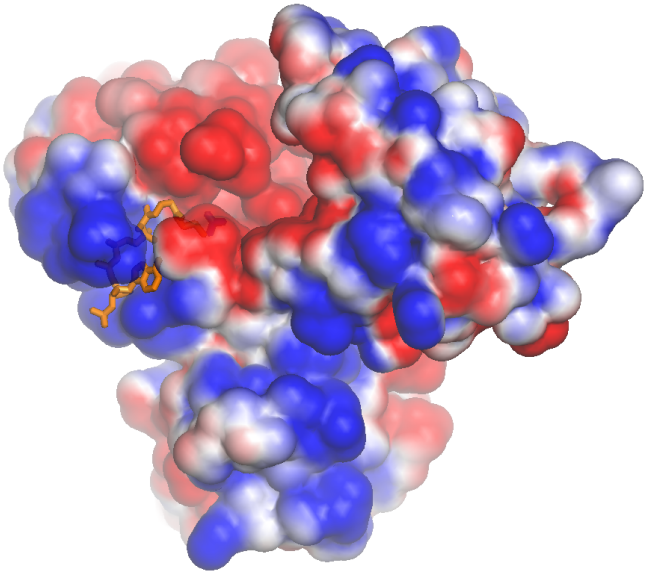

Fig. S14. The surface representation of the Eis monomer colored according to its electrostatic potential, positive in blue, negative in red, and hydrophobic in white.

6. Abbreviations

AAC, aminoglycoside acetyltransferase; AcCoA, acetyl-coenzyme A; AG, aminoglycoside; AMK, amikacin; APH, aminoglycoside phosphotransferase; APR, apramycin; CoA, coenzyme A; COSY, correlation spectroscopy; DEPT, distortionless enhancement by polarization; Eis, enhanced intracellular survival; GNAT, GCN5 related acetyltransferase; HETCOR, heteronuclear correlation experiment; FPLC, fast protein liquid chromatography; HYG, hygromycin; KAN, kanamycin A; LB, Luria-Bertani; LCMS, liquid chromatography mass spectrometry; MWCO, molecular weight cut-off; NEA, neamine; NEO, neomycin B; NET, netilmicin; PAR, paromomycin; R_f, retention factor; RIB, ribostamycin; SDS-PAGE, sodium dodecyl sulfate-polyacrylamide gel electrophoresis; SeMet, selenomethionine; SIS, sisomicin; SOE, splicing by overlapping extension; SPT, spectinomycin; STR, streptomycin; TLC, thin layer chromatography; TOB, tobramycin; TOCSY, total correlation spectroscopy.

7. References

1. Ho SN, Hunt HD, Horton RM, Pullen JK, & Pease LR (1989) Site-directed mutagenesis by overlap extension using the polymerase chain reaction. *Gene* 77(1):51-59.
2. Hegde SS, Javid-Majd F, & Blanchard JS (2001) Overexpression and mechanistic analysis of chromosomally encoded aminoglycoside 2'-N-acetyltransferase (AAC(2')-Ic) from *Mycobacterium tuberculosis*. *J Biol Chem* 276(49):45876-45881.

3. Vetting MW, Hegde SS, Javid-Majd F, Blanchard JS, & Roderick SL (2002) Aminoglycoside 2'-N-acetyltransferase from *Mycobacterium tuberculosis* in complex with coenzyme A and aminoglycoside substrates. *Nat Struct Biol* 9(9):653-658.
4. Green KD, Chen W, Houghton JL, Fridman M, & Garneau-Tsodikova S (2010) Exploring the substrate promiscuity of drug-modifying enzymes for the chemoenzymatic generation of N-acylated aminoglycosides. *Chembiochem* 11(1):119-126.
5. Magalhaes ML & Blanchard JS (2005) The kinetic mechanism of AAC3-IV aminoglycoside acetyltransferase from *Escherichia coli*. *Biochemistry* 44(49):16275-16283.
6. Dubois V*, et al.* (2002) Molecular characterization of a novel class 1 integron containing bla(GES-1) and a fused product of aac3-Ib/aac6'-Ib' gene cassettes in *Pseudomonas aeruginosa*. *Antimicrob Agents Chemother* 46(3):638-645.
7. Kim C, Villegas-Estrada A, Hesek D, & Mobashery S (2007) Mechanistic characterization of the bifunctional aminoglycoside-modifying enzyme AAC(3)-Ib/AAC(6')-Ib' from *Pseudomonas aeruginosa*. *Biochemistry* 46(17):5270-5282.
8. Boehr DD, Daigle DM, & Wright GD (2004) Domain-domain interactions in the aminoglycoside antibiotic resistance enzyme AAC(6')-APH(2"). *Biochemistry* 43(30):9846-9855.
9. Centron D & Roy PH (2002) Presence of a group II intron in a multiresistant *Serratia marcescens* strain that harbors three integrons and a novel gene fusion. *Antimicrob Agents Chemother* 46(5):1402-1409.
10. Kim C, Hesek D, Zajicek J, Vakulenko SB, & Mobashery S (2006) Characterization of the bifunctional aminoglycoside-modifying enzyme ANT(3")-Ii/AAC(6')-IId from *Serratia marcescens*. *Biochemistry* 45(27):8368-8377.
11. Andac CA, Stringfellow TC, Hornemann U, & Noyanalpan N (2011) NMR and amber analysis of the neamine pharmacophore for the design of novel aminoglycoside antibiotics. *Bioorg Chem* 39:28-41.
12. Park WKC, Auer M, Jaksche H, & Wong C-H (1996) Rapid combinatorial synthesis of aminoglycoside antibiotic mimetics: Use of a polyethylene glycol-inked amine and a neamine-derived aldehyde in multiple component condensation as a strategy for the discovery of new inhibitors of the HIV RNA Rev responsive element. *J Am Chem Soc* 118(42):10150-10155.
13. Otwinowski Z & Minor W (1997) Processing of X-ray Diffraction Data Collected in Oscillation Mode. *Methods in Enzymology, Macromolecular Crystallography, part A*, ed C.W. Carter JRMS, Eds. (Academic Press, New York), Vol 276, pp 307-326.
14. McCoy AJ*, et al.* (2007) Phaser crystallographic software. *J Appl Crystallogr* 40(Pt 4):658-674.
15. Emsley P & Cowtan K (2004) Coot: model-building tools for molecular graphics. *Acta Crystallogr D Biol Crystallogr* 60(Pt 12 Pt 1):2126-2132.
16. Murshudov GN, Vagin AA, & Dodson EJ (1997) Refinement of macromolecular structures by the maximum-likelihood method. *Acta Crystallogr D Biol Crystallogr* 53(Pt 3):240-255.
17. Vetting MW*, et al.* (2008) Mechanistic and structural analysis of aminoglycoside N-acetyltransferase AAC(6')-Ib and its bifunctional, fluoroquinolone-active AAC(6')-Ib-cr variant. *Biochemistry* 47(37):9825-9835.